Size effects on water adsorbed on hydrophobic probes at the nanometric scale

C. Calero, M. C. Gordillo, and J. Martí

Citation: J. Chem. Phys. **138**, 214702 (2013); doi: 10.1063/1.4807092
View online: http://dx.doi.org/10.1063/1.4807092
View Table of Contents: http://jcp.aip.org/resource/1/JCPSA6/v138/i21
Published by the American Institute of Physics.

Size effects on water adsorbed on hydrophobic probes at the nanometric scale

C. Calero,[1] M. C. Gordillo,[2] and J. Martí[1,a)]
[1]*Department of Physics and Nuclear Engineering, Technical University of Catalonia-Barcelona Tech, B4-B5 Northern Campus, Jordi Girona 1-3, 08034 Barcelona, Catalonia, Spain*
[2]*Departamento de Sistemas Físicos, Químicos y Naturales, Facultad de Ciencias Experimentales, Universidad Pablo de Olavide, Carretera de Utrera, km 1, 41013 Sevilla, Spain*

(Received 5 February 2013; accepted 24 April 2013; published online 3 June 2013)

Molecular dynamics simulations of liquid water at ambient conditions, adsorbed at the external walls of (n,n) single-walled armchair carbon nanotubes have been performed for $n = 5, 9, 12$. The comparison with the case of water adsorbed on graphene has also been included. The analysis of Helmholtz free energies reveals qualitatively different ranges of thermodynamical stability, eventually starting at a given threshold surface density. We observed that, in the framework of the force field considered here, water does not wet graphene nor (12,12) tubes, but it can coat thinner tubes such as (9,9) and (5,5), which indicates that the width of the carbon nanotube plays a role on wetting. On the other hand, density profiles, orientational distributions of water, and hydrogen-bond populations indicate significant changes of structure of water for the different surfaces. Further, we computed self-diffusion of water and spectral densities of water and carbon molecules, which again revealed different qualitative behavior of interfacial water depending on the size of the nanotube. The crossover size corresponds to tube diameters of around 1 nm. © *2013 AIP Publishing LLC*. [http://dx.doi.org/10.1063/1.4807092]

I. INTRODUCTION

In the last 20 years, the family of carbon forms has significantly grown with the discovery of fullerenes, carbon nanotubes, graphene, and other related structures. Mechanical, thermodynamical, and electrical properties of carbon nanotubes (CNTs) are unique.[1,2] In particular, chemical bonds in carbon nanotubes are entirely of the type sp^2, which gives them a unique strength and stiffness.[3] Such unique properties have recently inspired applications of great interest in several fields such as electronics,[4] physics of new materials,[5] or in electronic textile industry[6] to mention a few examples. The thinnest carbon nanotube is armchair (2,2) with a diameter of about 3 Å. This nanotube was grown inside a multi-walled CNT and was characterized by means of high-resolution transmission electron microscopy, Raman spectroscopy, and density functional theory calculations.[7] However, the thinnest freestanding single-walled CNTs are chiral ones, i.e., (n,m) with $n \neq m$ and have about 4.3 Å in diameter.[8] Other CNTs such as (3,3), (4,3), and (5,1) (all about 4 Å in diameter) have been identified using more precise aberration-corrected high-resolution transmission electron microscopy.[9]

Plenty of studies on water inside carbon nanotubes have been published (see Ref. 10 and references therein). The first molecular dynamics (MD) simulation of water inside single-walled CNT was reported in 2000,[11] where it was shown that water can access the interior of CNTs of radii large enough. Later, Hummer *et al.*[12] studied water conduction inside a nanotube, analyzing kinetics of filling and emptying. It was also found that the OH stretch spectral band split into two bands when water was inside CNT,[13] fact that was proposed as a method to measure tube radii and to perform CNT selection, since the spectral shift showed inverse proportionality to the tube radii. Experimental confirmation of this phenomenon was reported in 2004.[14] Finally, works by Walther *et al.*[15–17] reported contact angles for water inside CNT for several models and the existence of a breathing mode of CNT also proportional to inverse tube radius, in good agreement with experimental data.[18] Remarkably, a simulation of polarizable nanotubes immersed in water[19] indicated that polarization has only little effects compared to the electric field generated by the surrounding water. More recently findings include, to put only a few examples, effects of finite tube length on the phase diagram of CNT[20] or the use of electric fields to induce reversible wetting and dewetting of hydrophobic pores.[21] Furthermore, it has been obtained from MD simulations that water can spontaneously fill CNT simply by entropic forces.[22]

It is well known from the seminal work by Lee *et al.*[23] that properties of water at the interface with non-polar solutes are determined by the difficulty for water molecules to create hydrogen bonds. According to Chandler and co-workers,[24] depending on the size of the hydrophobic unit we can distinguish between two regimes. For small enough non-polar particles, water molecules can reorganize around them without sacrificing hydrogen bonds. Such structural change entails an entropic cost, which leads to low solubility of small non-polar species in water. Close to large non-polar solutes, the persistence of a hydrogen bond network is geometrically impossible, which makes water molecules move away from

a)Author to whom correspondence should be addressed. Electronic mail: jordi.marti@upc.edu

hydrophobic surfaces, producing thin vapor layers next to them (especially, if the liquid is close to coexistence with the vapor phase, as it is for water at ambient conditions). The crossover between these two regimes is predicted to be at sizes of about 1 nm.[24] In a recent experimental study,[25] Li and Walker have provided evidence confirming the existence of such a crossover in the dependence on the size of the solute of the hydration properties of single hydrophobic polymers. In the present study we have considered CNTs of different diameters as well as a flat graphene surface to ascertain the effect of the size of such hydrophobic solutes on the behavior of interfacial water. Since in the present work CNTs are not finite-sized solutes but periodic-sized probes, our aim will be to explore if they behave as large solutes and if there is any threshold size for such a behavior.

II. COMPUTATIONAL DETAILS

We considered liquid water adsorbed at the external surface of armchair single-walled CNTs of the type (n,n), with $n = 5, 9, 12$. In addition, simulations of bulk unconstrained water and of water adsorbed in flat graphene have been performed. In all cases we performed NVT simulations.

For each of the CNTs considered, a set of (about 10) simulations with different number of water molecules has been performed to analyze the thermodynamic stability of the water layer. Once determined the minimum surface density of water molecules needed to uniformly cover each of the CNT surfaces, we focused on the stable system with less water molecules and studied the structural and dynamical properties of the water layer. Characteristics of the selected stable systems are summarized in Table I.

Two snapshots of typical configurations for tubes (5,5) and (9,9) are depicted in Fig. 1. We highlight those water molecules located at shells closest to the nanotubes. The two most typical orientations of water at hydrophobic interfaces[26] can be observed, namely (1) dangling H-bonds, with oxygen-hydrogen molecular bonds pointing normally to the surface and (2) water molecules with instantaneous molecular planes roughly parallel to the surface of the tubes. These preferential orientations are common in water adsorbed at hydrophobic surfaces. A detailed analysis of orientational distributions will follow in Sec. III B.

Our simulation boxes were: $60.0 \times 60.0 \times 76.21$ Å^3 for water-(5,5)CNT system, $100.0 \times 100.0 \times 64.3$ Å^3 for water-(9,9)CNT, $150.0 \times 150.0 \times 83.35$ Å^3 for water-(12,12)CNT,

TABLE I. Characteristics of the selected stable systems studied in the present work: Tube length (l), tube diameter (D), and number of water molecules (N_w) considered in the simulations. In the case of graphene, the lengths are those of sides at the X-Y plane.

System	l (nm)	D (nm)	N_w
(5,5) CNT	7.62 (Z-axis)	0.66	835
(9,9) CNT	6.43 (Z-axis)	0.93	935
(12,12) CNT	8.33 (Z-axis)	1.13	4500
Graphene	3.19 × 3.40	...	1252
Bulk water	...	...	1000

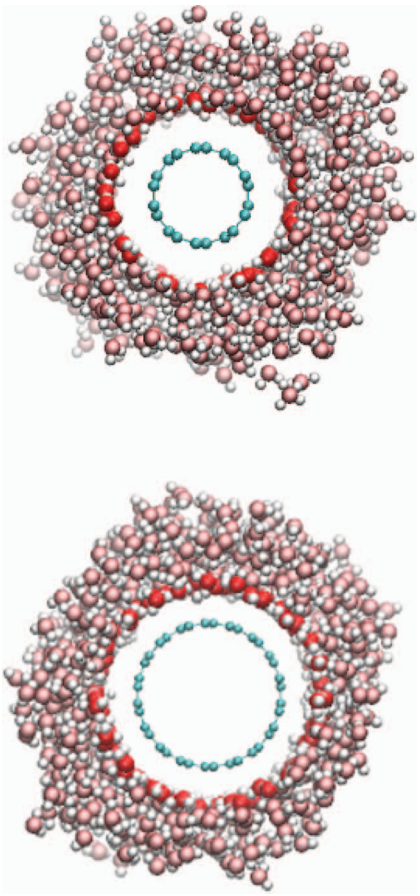

FIG. 1. Snapshots of two typical configurations of water adsorbed at the external surface of (5,5) (top) and (9,9) (bottom) carbon nanotubes. Tube's atoms are depicted in cyan, oxygens in white, and hydrogens in red. The atoms pertaining to the first water shell around the nanotubes are pictured in bright colors whereas remaining water have been shadowed.

and $31.929 \times 34.032 \times 40$ Å^3 for water-graphene, with periodicity along all three spatial directions. All carbon atoms were explicitly taken into account in the calculation and were considered to be rigid, i.e., the carbon atoms were not allowed to move in the simulation runs. This approximation was investigated in detail in a previous study,[27] which concluded that the mobility of carbons does not induce any noticeable change in the structure and dynamics of interfacial water. Nevertheless, a set of simulations with flexible armchair tubes and flexible graphene have been conducted to verify the rigid-carbon approximation and to compute vibrational spectra of carbons.

Initial configurations of the different systems were produced with the help of the 1.9 version of the Visual Molecular Dynamics software.[28] All simulations were performed using the NAMD-2.7 molecular dynamics package. Water-water and water-carbon interactions have been modeled by means of the CHARMM27 force field included in the package NAMD-2.7, especially designed for the simulation of biophysical systems.[29] The interactions concerning water and carbon are a combination of Coulomb interactions (water-water) with Lennard-Jones ones (water-water, water-carbon). Water has been modeled by using the TIP3P model.[30] The Lennard-Jones parameters for the water-carbon interaction

are $\sigma_{OC} = 3.350$ Å, $\epsilon_{OC} = 0.1032$ kcal/mol, $\sigma_{HC} = 1.975$ Å, and $\epsilon_{HC} = 0.0567$ kcal/mol. The long-ranged electrostatic interactions have been calculated by means of the particle mesh Ewald method.[31] The velocity Verlet algorithm has been used, together with temperature control using Langevin dynamics and a multiple time step methodology, with an integration time step of 0.5 fs for local interactions and another four times larger for long-ranged interactions. The equilibration in all cases ran for at least 100 ps, and the averages were calculated in runs of lengths longer than 1 ns.

III. RESULTS

A. Thermodynamic stability

In order to perform a meaningful study of the adsorption of water on the different CNTs and graphene, we need to establish the density limits of the thermodynamic stability of a coat of water on those substrates. A thermodynamically stable layer of water uniformly covers the substrate and no separation of denser and empty phases emerges. Since our MD simulations are performed at constant temperature, we need to calculate the free energy of the system and perform, if necessary, a Maxwell construction between the different phases to obtain those stability zones. However, the primary output of a classical MD simulation is the energy per particle, not the free energy. To estimate this last function, we used the same procedure than in previous works.[26,32] The scheme starts by proposing a functional form for the free energy which depends on the surface density ρ and temperature T, i.e., $F(\rho, T)$. We used

$$F(\rho, T) = \sum_{i=0}^{2} \sum_{j=1}^{3} b_{ij} \rho^i T^{1-j}, \tag{1}$$

where we have dropped the terms corresponding to an ideal gas. From the relation between the free energy and the energy

$$E = -T^2 \frac{\partial (F/T)}{\partial T}, \tag{2}$$

we can obtain a functional form for the energy whose parameters are the same b_{ij} coefficients that appear in Eq. (1). Thus, we can extract those parameters from a least squares fitting procedure to the energy per particle obtained directly from simulations at different densities and temperatures. Once the b_{ij} coefficients have been obtained, we substitute them back in Eq. (1) to compute the free energy. From the analysis of its dependence on density and temperature we can obtain the stability range of the adsorbed water layers. As it can be seen in Fig. 2, in which we display the energy versus the water density for the (5,5) and (9,9) tubes and graphene, the quality of the fits is very good, being the χ^2 values per degree of freedom less than one. This allowed us to limit the order of the density polynomial to two instead of the third-order polynomials used in Refs. 26 and 32. In addition, we only considered a single free energy function, since the energy per particle behaves monotonically as the water density increases. Such behavior is in contrast with the analysis performed in Ref. 32, where the appearance of two local minima in the energy dependence on density made necessary the use of two

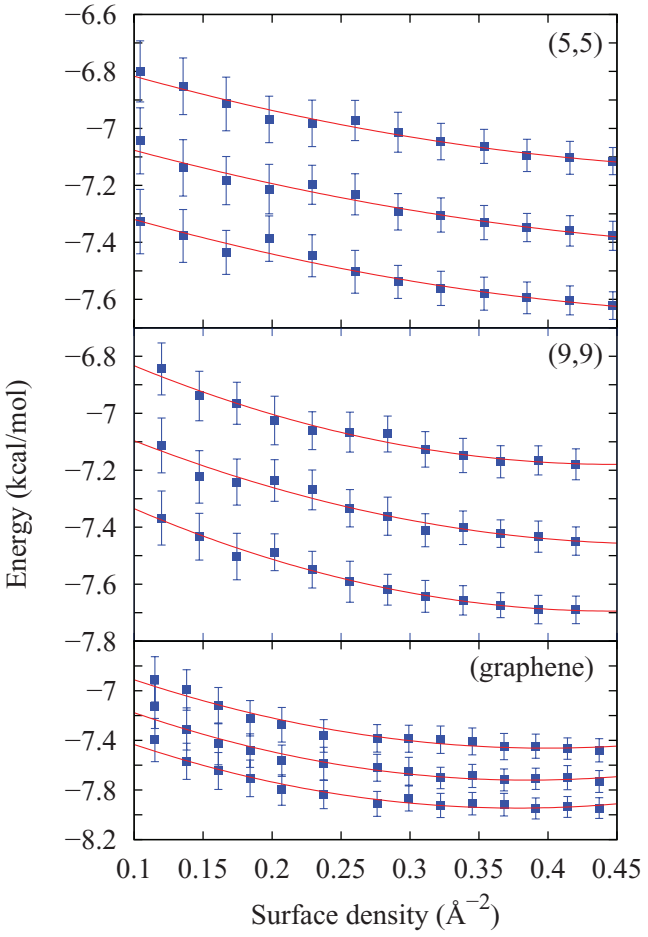

FIG. 2. Energy per water molecule in kcal/mol versus the surface density for three of the four system considered in this work. In all cases the lower curve corresponds to T = 298 K, the middle one to T = 310 K, and the upper set of results is that of T = 323 K. Full squares correspond to simulation results, while full lines are the results of least squares fits to Eq. (2).

independent fits in different density ranges. To calculate the water densities that appear in the abscissae of Fig. 2, we considered as a reference surface for the tubes cylinders whose lengths were those of their corresponding simulation cells and whose radii were given by the distance to the first peak of the radial density profile of water on those tubes (see below). In the case of graphene, densities were simply the number of molecules divided by the area of the flat surface.

From the least square fits of the data in Fig. 2 and from an equivalent set of results for the (12,12) tube, we obtained the free energy curves displayed in Fig. 3. Only the results for T = 298 K are given, being the curves corresponding to T = 310 and 323 K similar to those shown for each system, but displaced to lower values of the free energy per particle. Note that for the thinner tubes their corresponding free energy profiles have minima at ≈4.05 Å^2, corresponding to ∼905 and 790 water molecules for the (9,9) and (5,5) CNTs used in our simulations, respectively. Since the internal pressure of a system has to be positive to be stable, Fig. 3 indicates that the density of the water coat on those tubes has to be greater than 0.247 Å^{-2} (corresponding to the minima at 4.05 Å^2). In contrast, both for the (12,12) tube and the graphene surface, the minima of the free energy versus the inverse of the

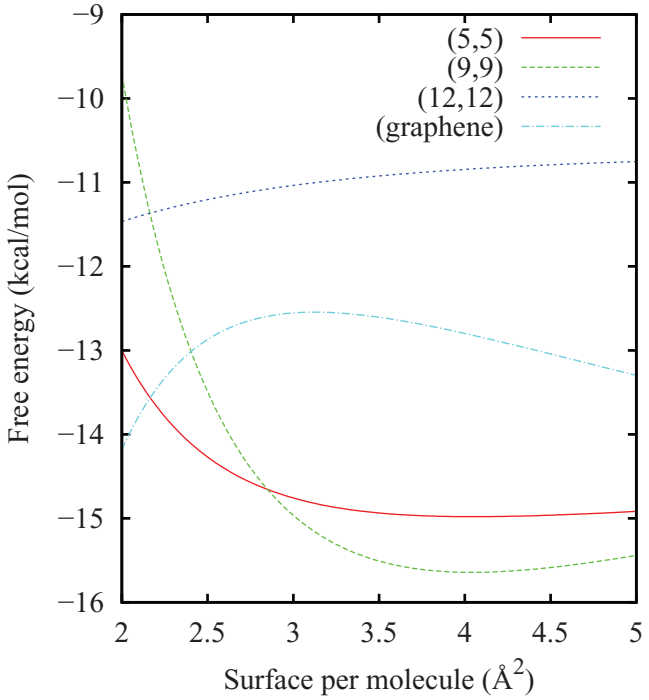

FIG. 3. Free energy per water molecule in kcal/mol versus the inverse of the surface density for the four systems considered in this work at T = 298 K, as deduced from Eqs. (1) and (2). In the thinner tubes minima are around 4.05 Å^2, while in the (12,12) tube and the graphene layer the minima are at the lowest surface per molecule considered.

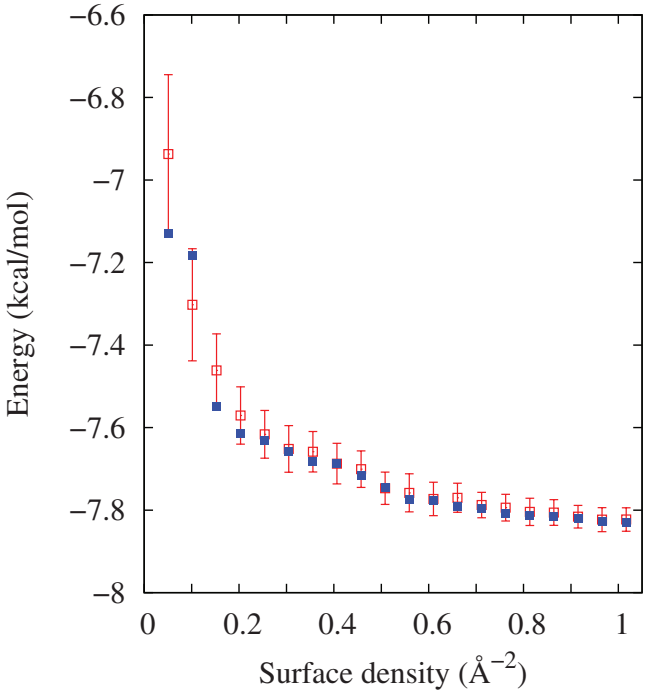

FIG. 4. Energy per water molecule, in kcal/mol as a function of the density outside a (12,12) tube at T = 298 K. Open symbols with error bars represent the results for the rigid water model, while full squares are the same results for a full flexible model once we have subtracted a contribution due to the vibrational degrees of freedom.

density is located at <2 Å^2. This means that the minimum free energy corresponds in both systems to a very thick coat of water on top of them, i.e., to bulk water surrounding the (12,12) tube and on top of graphene. This implies that, within the model used here, water does not wet either a (12,12) tube or a graphene surface. This result is consistent with the conclusions reported by Werder *et al.*[17] for a previous version of the CHARMM force field.

Water-graphite contact angles have been measured in different experiments,[33–36] producing angles in between 42° and 88°. If we consider that wetting occurs for angles lower than 90°, we conclude that water wets graphite. In the case of water on graphene, recent results[37,38] have been obtained for graphene films in solution coating different substrates (gold, highly-oriented-pyrolitic graphite, and copper). Depending on the substrate, contact angles for water on a single graphene layer range between 30° and 80°, always wetting the surface. In the present work, the simulated energies were calculated considering both the nanotube and water molecules as rigid bodies. This makes the lower part of Fig. 2 not directly comparable to the results of Ref. 26, in which a simple point charge (SPC) flexible water model (different from the one used in this work) was employed. In addition, rigidity makes the energy per water molecule decrease, since we are neglecting a positive energy contribution due to molecular vibrations. The different water models employed explain the different conclusion reached in a previous simulation work,[26] in which water wetted the graphene layer. The choice of the parameterization of the atomic interactions is thus critical to determine a surface's wetting properties.

We made sure that the introduction of the vibrational degrees of freedom both in the tube and in the water molecules did not change the thermodynamical analysis presented here. To prove it, we show the energy per water molecule as a function of density in Fig. 4 for a (12,12) tube at $T = 298$ K (the same behavior is found for the other two temperatures). Open symbols represent energy per water molecule for the case in which both water and tube are considered to be rigid. Full squares represent the energy per particle in the case of flexible water and carbon tube once a constant energy offset has been subtracted for all densities. This offset accounts for the vibrational energy of the carbon nanotube (2.22 ± 0.02 kcal/mol per carbon atom) and an additional difference of ∼1 kcal/mol for each water molecule. This energy is compatible with the difference between the energies of a single rigid water molecule (3.6 ± 1.6 kcal/mol) and a flexible one (1.8 ± 1.1 kcal/mol). The fact that this offset is constant for all energies means that, according to Eq. (2), its contribution to the free energy is a constant that does not change the position of the free energy minima nor the stability ranges indicated above.

B. Structure: Density profiles, hydrogen bonding, and water orientations

The structure of water adsorbed at the different CNTs is reported in Fig. 5. We calculated water density profiles by pinpointing the oxygen positions of each water molecule and the corresponding hydrogen-bond (HB) distributions. The HB definition assumed in the present work is a purely geometrical

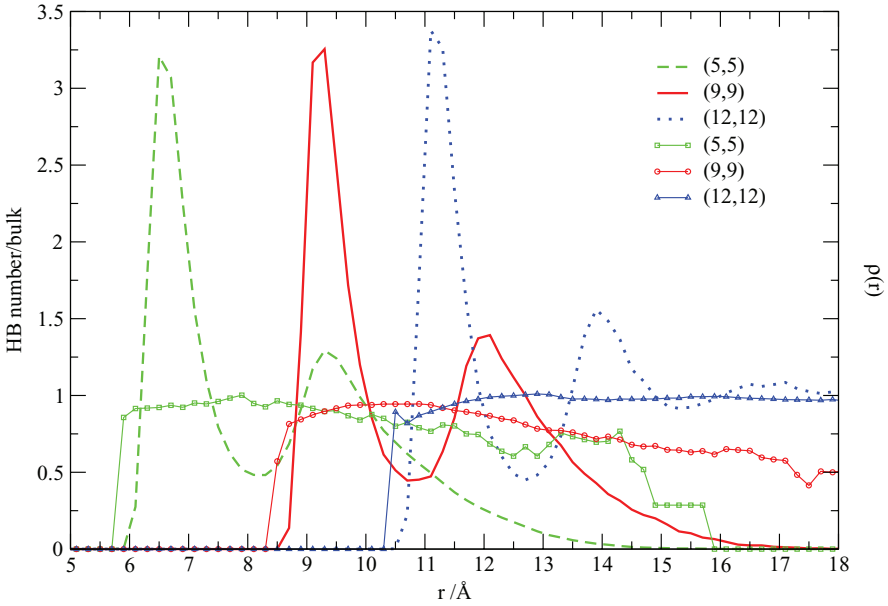

FIG. 5. Radial oxygen density profiles of water adsorbed at the external volume of CNT and hydrogen-bond populations as a function of radial distance at the center of the tubes.

one.[39] We consider two water molecules forming an HB when the oxygen-oxygen distance is smaller than 3.37 Å and the O–H–O angle is smaller than 30°. The cutoff for the O–O distance has been obtained from the position of the first minimum in oxygen-oxygen radial distribution functions obtained in bulk water simulations. The angular cutoff corresponds to the assumption that only quasi-linear HBs are accounted for, i.e., bifurcated and other kinds of HBs[40] have not been considered.

In all cases we observe a 2.7 Å width depletion region next to the tube surface, followed by an interfacial layer of water of about 2.5 Å of width, then a second water layer and finally a second interface formed by water and the vacuum. All such different regions are in shell-like radial structures, as can be seen in Fig. 1. The appearance of such interfacial structure is a well known feature for water near carbon-based structures.[41–43] Further, the structure of water adsorbed in paraffin-like plates[44] is very similar to the one reported in Fig. 5, which suggests that the key factor in determining water structure is the hydrophobic nature of the surface, independently of the particular arrangement of surface atoms.

The average number of HB per molecule $\langle n_{HB} \rangle$ is also reported. We obtained the normalized populations of HBs represented in Fig. 5 by dividing the number of HB by the corresponding bulk value for the force field used in the present work, which is about 3.7, very close to the experimental value of 3.9.[45] Here, we observe that normalized $\langle n_{HB} \rangle$ values start below 1 at tube-water interfaces in all cases. At longer radial distances, $\langle n_{HB} \rangle$ rises to values closer to the bulk value, to decrease again at water-vacuum interfaces. This is qualitatively similar to what happens in other hydrophobic surfaces, or in the particular case of flat and corrugated graphene, due to the existence of dangling bonds consisting of hydrogen atoms pointing directly to the surface.[43] In summary, the first water layer at the carbon nanotube interfaces is not able to form as many HBs as in bulk due to the existence of non-H-bonded hydrogens, but in the subsequent layers it can form almost as many hydrogen bonds as in bulk. Interestingly, we observe a bigger degree of H-bonding in the widest (12,12) tube.

This distribution of HB can be further understood by analyzing the orientation of water molecules at the interfaces. To do this, we computed the distribution of water dipole moment directions with respect to the normal to the carbon surface (not shown) by means of the two first Legendre polynomials considering as the relevant angle the one formed by the instantaneous dipole moment of water and the direction normal to the surface. The results obtained here simply corroborate previous findings and they can be summarized as follows: in all cases, water dipole moments tend to align parallel to CNTs' axial direction. This trend is very similar for all classes of tubes and it mainly accounts for dangling hydrogens, as reported above.[26,43] We also observed that the averaged angle between water dipole moment and the direction normal to interface is about $\cos\theta \sim 60°$, orientation that can be associated to configurations where the instantaneous molecular plane of water is roughly parallel to the surface of the CNT.[26]

C. Dynamics: Water diffusion and spectral densities of water and carbons

The diffusion of confined water is usually very different than that of bulk water.[46–48] Inside carbon slit-pores, for instance, when it is close to the walls, water diffuses in a different fashion than at the center of the structure,[49] tending to move along planes parallel to the carbon walls. In this work, we will present results for translational self-diffusion coefficients D_z of water oxygens computed along the CNT axial direction (Z-axis) compared to the bulk value. Diffusion along the radial direction was not considered because the large density reduction along such direction. Our calculations were made by means of the mean square displacement of

TABLE II. Dynamical properties of water adsorbed at CNTs: Diffusion coefficients in 10^{-5} cm^2/s and band maxima of water center-of-mass' spectral densities. All frequencies expressed in cm^{-1}. "HT" stands for hindered translations and "HB" stands for hydrogen-bond stretch.

CNT class	D_z	ω_{HT}	ω_{HB}
(5,5)	4.9	54	215
(9,9)	4.9	56	200
(12,12)	4.6	88	210
Graphene	4.6	80	215
Bulk unconstrained	5.8	41	200

oxygens and obtained from long-time slopes and by means of the Einstein's relationship. The results are presented in Table II for the three classes of CNTs and for graphene.

We observe that the water model considered in the present work overestimates water diffusion in bulk by a factor 2.5, since experimental value is close to 2.3 × 10^{-5} cm^2/s.[50] Assuming this drawback of the force field employed in the present work, we observe that diffusion coefficients of water computed alongside Z-axis are about 20% lower than that of the bulk unconstrained system. Of course this reduction is due to the presence of CNTs, even if we only consider axial diffusion. In previous works, we reported result of axial and normal diffusion of water at hydrophobic interfaces, revealing that water's translational diffusion is essentially due to motion along the first interfacial layer, with values of normal diffusion reduced in about one order of magnitude.[51,52] Most noticeable is the fact that no significant changes are found when different CNTs are considered: in all cases the reduction of the diffusion is almost of the same magnitude. This seems to indicate that, in a similar fashion as it happens with the structural properties studied, dynamics is not essentially affected by the size of the probe.

However, a different behavior is observed when probing the vibrational properties (such as the absorption spectra) of interfacial water at the different carbon nanotubes. There is a quite simple and elegant way to do this in MD simulations of aqueous systems, namely the calculation of Fourier transform spectral densities from atomic velocity autocorrelation functions. This is a standard procedure which reveals valuable information on microscopical vibrational modes.[53] In the present case, we have compared spectral densities from center-of-mass velocities of water at different interfaces with the case of the bulk unconstrained system. We present results in Fig. 6, together with a summary of the main findings in Table II. All these results have been obtained from simulations where CNTs have been considered as rigid, not allowing vibrations of carbon atoms.

The relevant trend is the existence of spectral shifts for two specific vibrations. Experimental measurements have reported the same two main bands centered at about 60 and 200 cm^{-1} (see Ref. 54 and references therein for a detailed discussion about their physical meaning). These bands have been attributed to restricted translations of water inside the cage of neighboring molecules called *rattling in a cage* (with a peak at about 60 wavenumbers) and to the signature of HB stretching vibrations (shoulder centered around 200 cm^{-1}). In

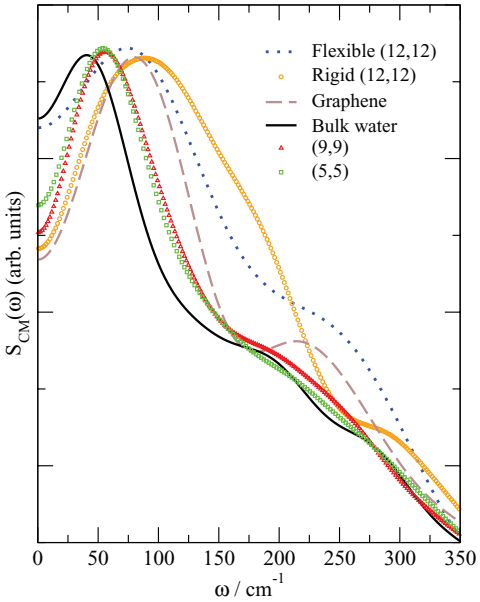

FIG. 6. Water center-of-mass spectral densities computed from Fourier transforms of center-of-mass velocity autocorrelation functions. Only the (12,12) CNT has been considered either made with rigid or flexible bonds, whereas tubes (5,5) and (9,9) have rigid bonds.

our case, bulk values are located at ∼40 and ∼200 cm^{-1}, in an overall good agreement with experimental data.

For water at the interface with the different CNTs, the high-frequency spectra around 200 cm^{-1} is unchanged with respect to the bulk, since it is essentially due to water-water vibrations through HBs and not connected to collective modes such as cage-vibrations associated with the 40 cm^{-1} band. When analyzing this latter low-frequency band we observe a blueshift with respect to the bulk water value case of about 15 cm^{-1} when narrow tubes—(5,5) and (9,9)—are considered, whereas this shift is significantly bigger, of about 40 cm^{-1}, for larger species such as the (12,12) tube or a flat graphene sheet. For the (12,12) case, we tested the effect on the water spectra of considering rigid carbon surfaces. We compared the spectra of water shown in Fig. 6, obtained from simulations with rigid CNTs, and the spectra of water obtained from independent simulations considering flexible carbon surfaces. Whereas the high frequency band remains unaltered, the difference in the low frequency band shift between the rigid and flexible cases is about 25% of the total shift with respect to the bulk water system. Thus, we can infer from our results that it is the curvature of the adsorbing surface the main factor inducing the spectral shifts, and that within the systems considered we can clearly distinguish two groups with respect to their effect on the spectral shift: one for the thin tubes such as (5,5) and (9,9) and a second one for the tube (12,12) and the flat graphene sheet. The crossover size is in between the diameters of the (9,9) and (12,12) tubes, i.e., around 1 nm. Such different behavior for different tube diameters could be an indication of the two regimes of hydration around hydrophobic apolar species proposed by Lum, Chandler, and Weeks.[24] According to their view, water molecules can restructure to preserve the hydrogen bond network when

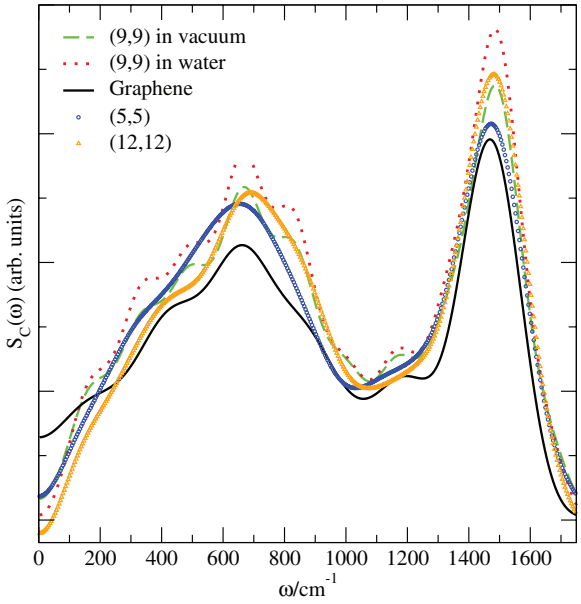

FIG. 7. Carbon spectral densities computed from Fourier transforms of carbon velocity autocorrelation functions. Here the (9,9) CNTs have been considered either in vacuum or in water whereas tubes (12,12) and (5,5) were in vacuum.

hydrating nonpolar solutes smaller than 1 nm, but they are unable to do so for bigger hydrophobes.

Finally, Fig. 7 reports the absorption spectra of carbons for bare and water-coated tubes, in an effort to analyze the influence of the environment on the vibrational motions of carbons. To do this, we performed a series of additional simulations of aqueous tubes and for tubes in vacuum, where carbon vibrations were allowed. In these cases (see Fig. 4), the stability regimes were the same as those obtained for water adsorbed at rigid tubes. From our results, we can highlight several features. On the one hand, we observe two main bands corresponding to vibrations at 665 and 1480 cm^{-1} in all cases, i.e., for narrow (5,5) and thick (12,12) tubes as well as for the intermediate ones (9,9) and for graphene, with only little shifts observed, regardless of the tube radii. Further, the two vibrational modes of carbons obtained are centered at the same values for aqueous and isolated tubes, regardless of the hydration degree. This indicates that carbon vibrations are not affected by the adsorbed water at the CNTs. In addition, the two modes have been obtained with good qualitative agreement with experimental data. Indeed, there is general agreement of the existence of a weak and a strong bands in the regions of 800–900 and 1500–1600 cm^{-1}, respectively.[55–57] This can be considered as a strong indication of the validity of the present force field to model correctly carbon interactions.

IV. CONCLUDING REMARKS

We have simulated liquid water at ambient conditions adsorbed at the external walls of several armchair CNT, with diameters between 0.27 and 1.18 nm, by means of classical MD simulations. The calculation of the thermodynamically stable regions indicated that for all classes of CNT only one single region in the phase diagram exists for each CNT, defined by a given threshold surface density. For the potential models employed in the present work, different behavior has been obtained. So, whereas flat graphene or thick CNTs such as (12,12) are not coated by water, thin tubes (9,9) and (5,5) are fully coated.

The effects of the presence of large species on water structure are relevant at the carbon-water interface, where some hydrogen-bonds are broken and two particular water arrangements (dangling hydrogens, waters with molecular plane parallel to the local surface of the tubes) have been identified. However, no significant differences arose for CNTs of different diameter. Conversely, subtle effects on the water absorption spectra when comparing large to small hydrophobic probes have been obtained. At the mid-infrared spectral region, spectral densities of states computed through Fourier transforms of center-of-mass water velocity autocorrelation functions, we obtained significant frequency blueshifts (taking the values of unconstrained water as the reference) for hindered translational modes. This may indicate that large individual apolar species mainly affect vibrational motions, keeping the structure of the hydrogen-bond network essentially unchanged. As a validation of the force field used in this work, carbon vibrational frequencies have been correctly reproduced by the simulations.

ACKNOWLEDGMENTS

M.C.G. thanks the "Ministerio de Ciencia e Innovación" of Spain (MICINN) for financial support under Grant No. FIS2010-18356 and the *Junta de Andalucia* (Group PAI-205 and Grant No. FQM-5985). C.C. and J.M. gratefully acknowledge financial support from the *Direcció General de Recerca de la Generalitat de Catalunya* (Grant No. 2009-SGR-1003) and the Spanish MICINN for Grant No. FIS2012-39443-C02-01. C.C. is a UPC post-doctoral fellow.

[1]R. Saito, G. Dresselhaus, and M. S. Dresselhaus, *Physical Properties of Carbon Nanotubes* (Imperial College, London, UK, 1998).
[2]T. W. Odom, J.-L. Huang, P. Kim, and C. M. Lieber, J. Phys. Chem. B **104**, 2794 (2000).
[3]M.-F. Yu, O. Lourie, M. J. Dyer, K. Moloni, T. F. Kelly, and R. S. Ruoff, Science **287**, 637 (2000).
[4]Z. Chen, J. Appenzeller, Y.-M. Lin, J. Sippel-Oakley, A. G. Rinzler, J. Tang, S. J. Wind, P. M. Solomon, and P. Avouris, Science **311**, 1735 (2006).
[5]A. E. Aliev, J. Oh, M. E. Kozlov, A. A. Kuznetsov, S. Fang, A. F. Fonseca, R. Ovalle, M. D. Lima, M. H. Haque, Y. N. Gartstein, M. Zhang, A. A. Zakhidov, and R. H. Baughman, Science **323**, 1575 (2009).
[6]A. B. Dalton, S. Collins, E. Muñoz, J. M. Razal, V. H. Ebron, J. P. Ferraris, J. N. Coleman, B. G. Kim, and R. H. Baughman, Nature (London) **423**, 703 (2003).
[7]X. Zhao, Y. Liu, S. Inoue, T. Suzuki, R. Jones, and Y. Ando, Phys. Rev. Lett. **92**, 125502 (2004).
[8]T. Hayashi, Y. A. Kim, T. Matoba, M. Esaka, K. Nishimura, T. Tsukada, M. Endo, and M. S. Dresselhaus, Nano Lett. **3**, 887 (2003).
[9]L. Guan, K. Suenaga, and S. Iijima, Nano Lett. **8**, 459 (2008).
[10]A. Alexiadis and S. Kassinos, Chem. Rev. **108**, 5014 (2008).
[11]M. C. Gordillo and J. Martí, Chem. Phys. Lett. **329**, 341 (2000).
[12]G. Hummer, J. C. Rasaiah, and J. P. Noworyta, Nature (London) **414**, 188 (2001).
[13]J. Martí and M. C. Gordillo, Phys. Rev. B **63**, 165430 (2001).
[14]A. I. Kolesnikov, J.-M. Zanotti, C.-K. Loong, and P. Thiyagarajan, Phys. Rev. Lett. **93**, 035503 (2004).
[15]T. Werder, J. H. Walther, R. L. Jaffe, T. Halicioglu, F. Noca, and P. Koumoutsakos, Nano Lett. **1**, 697 (2001).

[16]J. H. Walther, R. L. Jaffe, T. Halicioglu, and P. Koumoutsakos, J. Phys. Chem. B **105**, 9980 (2001).
[17]T. Werder, J. H. Walther, R. L. Jaffe, T. Halicioglu, and P. Koumoutsakos, J. Phys. Chem. B **107**, 1345 (2003).
[18]G. S. Duesberg, W. J. Blau, H. J. Byrne, J. Muster, M. Burghard, S. Roth, Chem. Phys. Lett. **310**, 8 (1999).
[19]F. Moulin, M. Devel, and S. Picaud, Phys. Rev. B **71**, 165401 (2005).
[20]H. Kyakuno, K. Matsuda, H. Yahiro, Y. Inami, T. Fukuoka, Y. Miyata, K. Yanagi, Y. Maniwa, H. Kataura, T. Saito, M. Yumura, and S. Iijima, J. Chem. Phys. **134**, 244501 (2011).
[21]M. R. Powell, L. Cleary, M. Davenport, K. J. Shea, and Z. S. Siwy, Nat. Nanotechnol. **6**, 798 (2011).
[22]T. A. Pascal, W. A. Goddard, and Y. Jung, Proc. Natl. Acad. Sci. U.S.A. **108**, 11794 (2011).
[23]C. Y. Lee, J. A. McCammon, and P. J. Rossky, J. Chem. Phys. **80**, 4448 (1984).
[24]K. Lum, D. Chandler, and J. D. Weeks, J. Phys. Chem. B **103**, 4570 (1999).
[25]I. T. S. Li and G. C. Walker, Proc. Natl. Acad. Sci. U.S.A. **108**, 16527 (2011).
[26]M. C. Gordillo and J. Martí, Phys. Rev. B **78**, 075432 (2008).
[27]M. C. Gordillo and J. Martí, J. Phys. Chem. B **114**, 4583 (2010).
[28]W. Humphrey, A. Dalke, and K. Schulten, J. Mol. Graphics **14**, 33 (1996).
[29]J. C. Phillips, R. Braun, W. Wang, J. Gumbart, E. Tajkhorshid, E. Villa, C. Chipot, R. D. Skeel, L. Kale, and K. Schulten, J. Comput. Chem. **26**, 1781 (2005).
[30]W. L. Jorgensen, J. Chandrasekhar, J. D. Madura, R. W. Impey, and M. L. Klein, J. Chem. Phys. **79**, 926 (1983).
[31]T. Darden, T. York, and L. Pedersen, J. Chem. Phys. **98**, 10089 (1993).
[32]M. C. Gordillo and J. Martí, Phys. Rev. B **67**, 205425 (2003).
[33]F. M. Fowkes and W. D. Harkins, J. Am. Chem. Soc. **62**, 3377 (1940).
[34]I. Morcos, J. Chem. Phys. **57**, 1801 (1972).
[35]M. E. Tadros, P. Hu, and A. W. Adamson, J. Colloid Interface Sci. **49**, 184 (1974).
[36]M. E. Schrader, J. Phys. Chem. **84**, 2774 (1980).
[37]J. Rafiee, M. A. Rafiee, Z.-Z. Yu, and N. Koratkar, Adv. Mater. **22**, 2151 (2010).
[38]J. Rafiee, X. Mi, H. Gullapalli, A. V. Thomas, F. Yavari, Y. Shi, P. M. Ajayan, and N. A. Koratkar, Nature Mater. **11**, 217 (2012).
[39]J. Martí, Phys. Rev. E **61**, 449 (2000).
[40]M. Boero, K. Terakura, T. Ikeshoji, C. C. Liew, and M. Parrinello, Phys. Rev. Lett. **85**, 3245 (2000).
[41]J. Martí, G. Nagy, M. C. Gordillo, and E. Guàrdia, J. Chem. Phys. **124**, 094703 (2006).
[42]G. Nagy, M. C. Gordillo, E. Guàrdia, and J. Martí, J. Phys. Chem. B **111**, 12524 (2007).
[43]G. Cicero, J. K. Grossman, E. Schwegler, F. Gygi, and G. Galli, J. Am. Chem. Soc. **130**, 1871 (2008).
[44]N. Choudhury, J. Phys. Chem. B **112**, 6296 (2008).
[45]N. Matubayashi, C. Wakai, and M. Nakahara, J. Chem. Phys. **107**, 9133 (1997).
[46]J. J. Gilijamse, A. J. Lock, and H. J. Bakker, Proc. Natl. Acad. Sci. U.S.A. **102**, 3202 (2005).
[47]N. Choudhury and B. M. Pettitt, J. Phys. Chem. B **109**, 6422 (2005).
[48]N. R. Tummala and A. Striolo, J. Phys. Chem. B **112**, 10675 (2008).
[49]J. Martí, G. Nagy, M. C. Gordillo, and E. Guàrdia, J. Phys. Chem. B **110**, 23987 (2006).
[50]R. Hausser, G. Maier, and F. Noack, Z. Naturforsch. A **21**, 1410 (1966).
[51]J. Martí and M. C. Gordillo, J. Chem. Phys. **119**, 12540 (2003).
[52]J. Martí, J. Sala, and E. Guàrdia, J. Mol. Liq. **153**, 72 (2009).
[53]J. Martí, E. Guàrdia, and J. A. Padró, J. Chem. Phys. **101**, 10883 (1994).
[54]J. A. Padró and J. Martí, J. Chem. Phys. **120**, 1659 (2004).
[55]U. Kuhlmann, H. Jantoljak, N. Pfander, P. Bernier, C. Journet, and C. Thomsen, Chem. Phys. Lett. **294**, 237 (1998).
[56]K. Sbai, A. Rahmani, H. Chadli, J.-L. Bantignies, P. Hermet, and J.-L. Sauvajol, J. Phys. Chem. B **110**, 12388 (2006).
[57]J.-L. Bantignies, J.-L. Sauvajol, A. Rahmani, and E. Flahaut, Phys. Rev. B **74**, 195425 (2006).